Magnetization steps in $Pb_{1-x}Eu_xS$: Exchange and anisotropic interactions

Valdir Bindilatti, Ewout ter Haar, and Nei F. Oliveira, Jr.
Instituto de Física, Universidade de São Paulo, Caixa Postal 66318, CEP 05315-970 São Paulo, SP, Brazil

M. T. Liu and Y. Shapira
Department of Physics and Astronomy, Tufts University, Medford, Massachusetts 02155

X. Gratens, S. Charar, S. Isber, P. Masri, and M. Averous
Groupe d'Etude des Semiconducteurs URA 357, Université Montpellier II, Place Eugene Bataillon, 34095 Montpellier Cedex 5, France

Z. Golacki
Institute of Physics, Polish Academy of Sciences, Pl. 02-668 Warsaw, Poland

E. J. McNiff, Jr.
Francis Bitter National Magnet Laboratory, Massachusetts Institute of Technology, Cambridge, Massachusetts 02139
(Received 25 August 1997)

Magnetization measurements were performed on five $Pb_{1-x}Eu_xS$ samples, with $0.0092 \leqslant x \leqslant 0.059$. Two of the samples were measured at 20 mK in magnetic fields **H** up to 50 kOe parallel to the [111] and [100] directions. The other three samples were measured at 0.6 K in fields up to 180 kOe. The 20 mK data exhibit magnetization steps (MST's) arising from pairs. These MST's depend on the direction of **H**, so that anisotropic interactions must be included in the data analysis. The MST's lead to a value $J/k_B = -0.228 \pm 0.007$ K for the dominant antiferromagnetic exchange constant. Computer simulations identify this J as the nearest-neighbor exchange constant J_1, and show that the Eu distribution over the cation sites is random or very nearly random. The MST's from pairs exhibit a splitting when **H** is parallel to [100]. The splitting is tentatively attributed to exchange anisotropy, in which case the above value for J refers to the average exchange constant $\overline{J}$. The 20 mK data for $\mathbf{H} \| [100]$ also show a MST from isolated Eu ions. This MST occurs because such ''singles'' are subjected to a cubic crystal-field anisotropy. [S0163-1829(98)03813-2]

I. INTRODUCTION

In the last decade magnetization steps (MST's) have been used to measure antiferromagnetic (AF) exchange constants between the magnetic ions in dilute magnetic semiconductors (DMS's). Early works[1] focused on Mn-based II-VI DMS's, with a typical value of -10 K for the dominant Mn-Mn exchange constant J. More recently the Eu-Eu exchange interaction has been studied in $Pb_{1-x}Eu_xSe$ and $Pb_{1-x}Eu_xTe$.[2,3] The present work on $Pb_{1-x}Eu_xS$ continues the study of lead salts containing Eu, which are important examples of IV-VI DMS's.[4] In the lead salts even the largest Eu-Eu exchange constant is only of order -0.1 K. To determine such a small J it was necessary to change the experimental techniques. The temperature requirement $k_BT \ll |J|$ for resolving the MST's mandates the use of a dilution refrigerator and a magnetometer capable of operating at these very low temperatures.[5]

On the theoretical side, a simple model with one exchange constant J and with no anisotropy was adequate for the early studies of MST's in Mn-based II-VI DMS's.[1] Models with more than one exchange constant were developed later.[6,7] Anisotropy is usually unimportant for MST's involving Mn^{2+} ions, but it was considered for MST's involving Fe^{2+}, Co^{2+}, and Cr^{2+} ions.[8–10] In the present work on Eu^{2+} ions in $Pb_{1-x}Eu_xS$ it was essential to include anisotropic interactions in theoretical modeling of the low-temperature magnetization curves. Although the Eu^{2+} ion, like Mn^{2+}, is an S-state ion with a typically small anisotropy, the exchange interactions between the Eu ions are so weak that even small anisotropies are important.

The lead salts have the rocksalt structure. The cubic crystal-field anisotropy for isolated Eu^{2+} ions in these materials was studied by EPR.[11] This anisotropy is largest for Eu^{2+} in PbS, smaller for Eu^{2+} in PbSe (roughly by a factor of 2), and smaller still for Eu^{2+} in PbTe (another factor of 2). The effects of this anisotropy on the MST's were considered briefly in the work on $Pb_{1-x}Eu_xSe$,[2] but because of their small size they were largely ignored in $Pb_{1-x}Eu_xTe$.[3] In the present work on $Pb_{1-x}Eu_xS$ it was essential to include the single-ion cubic anisotropy.

The cubic crystal-field anisotropy is the only anisotropy for isolated ions. For Eu ions which are in pairs, or in larger clusters, several other anisotropies may be important.[12–14] One of these arises from the fact that in such clusters the local environment for each Eu ion is no longer cubic. Noncubic crystal-field terms may then be needed. Another anisotropy arises from the dipole-dipole interaction. Finally, the exchange interaction itself can be anisotropic. These additional anisotropies were ignored in the earlier papers,[2,3] but had to be considered in the present work because of the discovery of a splitting of the MST's.

The main themes of this paper are (1) the determination of the dominant AF exchange constant J, (2) the identification

of this J as the nearest-neighbor (NN) exchange constant, (3) the splitting of the MST's arising from pairs, and (4) the large MST which arises from isolated Eu ions (singles). The importance of the anisotropies is emphasized throughout.

II. THEORY

Some of the theory for the present work was discussed earlier.[1–3,15] Models with one exchange constant J, which is AF, prove adequate for the present study. In such models the spins in a DMS are divided into clusters: singles, pairs, open triplets (OT's), closed triplets (CT's), and six types of quartets. Spins in clusters larger than quartets are collectively referred to as ''others.'' The magnetization of each cluster type can be calculated, and the total magnetization is obtained by summing over all the clusters. To perform the latter sum one usually assumes that the Eu ions are randomly distributed over the cation sites. The statistics of the clusters is then known.[16] The contribution of clusters larger than quartets to the magnetization curve is usually quite small, so that a rough approximation for these others is adequate. This approximation was discussed in Ref. 3.

In the simplest model, only one isotropic exchange constant J and the Zeeman energy are included, but all anisotropies are neglected. We shall refer to this model as $1J$-0 (one J, zero anisotropy). Extensive discussions of this model have already been given.[1–3,15] Here, we emphasize the effects resulting from various anisotropies.

A. Cubic crystal-field anisotropy

Among all the anisotropies in $Pb_{1-x}Eu_xS$ the one due to the cubic crystal field acting on each Eu ion has the largest effect on the magnetization. The Hamiltonian for this cubic anisotropy was discussed by Abragam and Bleaney.[17] The relevant anisotropy parameters for Eu^{2+} ions in PbS are $b_4=0.459$ GHz and $b_6=-0.0015$ GHz. The g factor is 1.975. These values are from electron paramagnetic resonance (EPR).[11] The model in which only one isotropic exchange constant and the cubic crystal field are included will be referred to as the $1J$-CUB model. Such a model was briefly considered in Ref. 2, but since the effects of the cubic crystal field are much stronger in the present system, a more extensive treatment is warranted.

1. Singles

For the Eu concentrations in the present work $x \leqslant 0.059$ the number of spins which are singles exceeds the number in any other cluster type. Including the cubic crystal field but excluding all other anisotropies is very realistic for singles because other anisotropies exist only when there are neighboring Eu ions. The main effect of the cubic anisotropy is to slow down the alignment of the singles in a magnetic field **H**. This slowing down is important well below 1 K where the thermal energy k_BT is smaller than the level splitting caused by the cubic crystal field.

The most spectacular effect occurs when **H** is parallel to one of the $\langle 100 \rangle$ crystal axes. The cubic anisotropy then leads to a large MST from the singles. The energy-level crossing causing this MST is shown in the inset of Fig. 1. The MST should occur at $H_c=3.38$ kOe, and it should lead

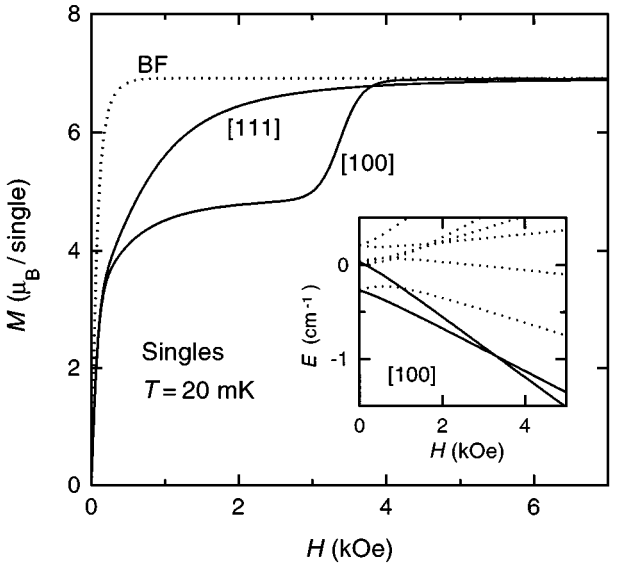

FIG. 1. Calculated magnetization M of Eu^{2+} singles in $Pb_{1-x}Eu_xS$ at $T=20$ mK. The solid curves for $\mathbf{H}\|[100]$ and $\mathbf{H}\|[111]$ use the cubic crystal-field anisotropy parameters $b_4=0.459$ GHz, $b_6=-0.0015$ GHz, and $g=1.975$. The dotted line is the Brillouin function (BF), which applies when there is no anisotropy. The inset shows the energy levels of a single for $\mathbf{H}\|[100]$. The crossing of the two levels shown as solid lines leads to the step in the magnetization curve.

to an increase of the magnetization M by a factor of about 7/5. The MST disappears when **H** is not close to any of the $\langle 100 \rangle$ directions because the level crossing changes to anticrossing.

Figure 1 shows the predicted magnetization of singles at 20 mK for both $\mathbf{H}\|[100]$ and $\mathbf{H}\|[111]$. These results are based on the $1J$-CUB model. The dotted line in Fig. 1 is the prediction of the $1J$-0 model (i.e., a Brillouin function). Clearly, the cubic anisotropy causes the singles' magnetization to saturate at a higher field.

2. Pairs

Except for singles, which are not affected by J, pairs are the most numerous clusters. Information concerning J is therefore obtained largely from the pairs' response. In the $1J$-0 model the Eu-pairs give rise to seven MST's at low temperatures ($k_BT \ll |J|$).[1–3] These MST's are equally spaced, and they occur at fields H_n which are given by

$$g\mu_B H_n = 2|J|n, \tag{1}$$

where $n=1,2,\ldots,7$. The overall appearance of the magnetization curve for pairs is that of a ''ramp'' composed of seven steps. The ramp ends at $H \simeq 14|J|/g\mu_B$, when the pairs' magnetization becomes saturated.

The energy levels of a pair when cubic anisotropy is also included were obtained by a numerical diagonalization of the Hamiltonian matrix. The magnetization M was then obtained via the partition function. The qualitative features (a ramp composed of seven MST's) remain the same. However, the MST's are no longer equally spaced, and the positions of the MST's and the average spacing between them depend on the direction of **H**. These effects of the cubic anisotropy are

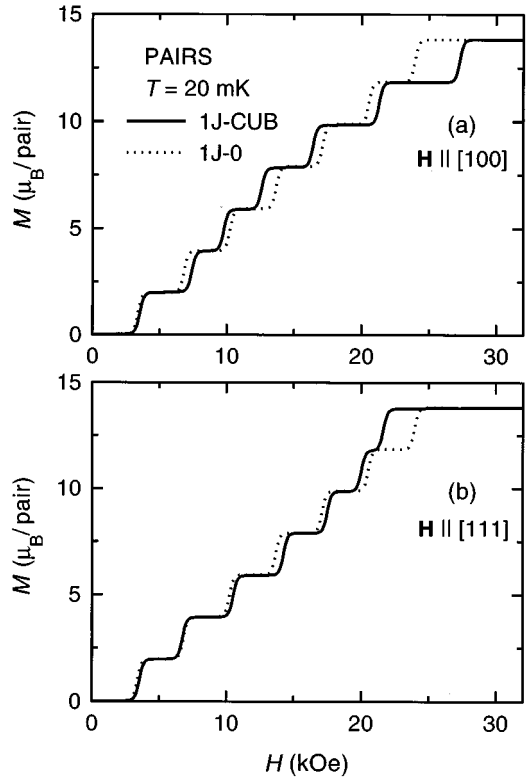

FIG. 2. Calculated magnetization of Eu^{2+} pairs in $Pb_{1-x}Eu_xS$ at $T=20$ mK. (a) $\mathbf{H}||[100]$, (b) $\mathbf{H}||[111]$. The solid curves are based on the $1J$-CUB model, i.e., one exchange constant and the cubic crystal-field anisotropy. The dotted curve, which is the same in both parts of the figure, uses the $1J$-0 model (one J, no anisotropy).

quite strong for the parameters of $Pb_{1-x}Eu_xS$ (b_4, b_6, and g as given above, and $J/k_B=-0.228$ K from the data analysis below).

The solid curves in Fig. 2 show the pair magnetization calculated from the $1J$-CUB model for $\mathbf{H}||[100]$ and $\mathbf{H}||[111]$. These results for $T=20$ mK used the parameters for $Pb_{1-x}Eu_xS$. The dotted curves are for zero anisotropy ($1J$-0 model). The cubic anisotropy causes the ramp for $\mathbf{H}||[111]$ to end at a significantly lower field than for $\mathbf{H}||[100]$. For either field direction the six separations $\Delta H=H_{n+1}-H_n$ between successive MST's are unequal. When $\mathbf{H}||[100]$ the separation between the sixth and seventh steps is the largest among the six separations. For $\mathbf{H}||[111]$ the separation between the sixth and seventh steps is the smallest.

3. Triplets

For Eu concentrations $x\leqslant 0.059$, significantly fewer spins are in triplets than in pairs. Among the two types of triplets, there are many more OT's than CT's. The ground state of either type of triplet has a net moment which aligns readily in a field. Calculations using the $1J$-0 model[2] show that for either type of triplet, a ramp composed of equally spaced MST's appears at high H if T is sufficiently low. The ramp for OT's consists of seven MST's, the first at $g\mu_BH=9|J|$ and the last at $g\mu_BH=21|J|$. The ramp for CT's consists of ten MST's, the first at $g\mu_BH=3|J|$ and the last at $g\mu_BH=21|J|$. Note that the ramps for both CT's and OT's end at the same field. This field is 50% higher than the field at which the pairs' ramp ends.

The simple $1J$-0 model already indicates the difficulties of observing the ramps (or MST's) from CT's and OT's. Triplets are not the only contributors to the magnetization. When x is of order 0.01 the slope of the pairs' ramp is much higher than those of the triplets' ramps. Therefore, in the field region where the pairs' ramp overlaps the triplets' ramps, the pairs' ramp dominates. The combined triplets' ramp, due to both OT's and CT's, becomes apparent only after the pairs' ramp ends.

Inclusion of the cubic anisotropy does not change the qualitative features of the MST's arising from OT's and CT's. The energy levels of both types of triplet were obtained from the $1J$-CUB model by a numerical diagonalization of the Hamiltonian matrix. The calculations were for $\mathbf{H}||[100]$ and $\mathbf{H}||[111]$. The magnetization was then calculated via the partition function. Due to the cubic anisotropy the MST's are no longer equally spaced, and the fields where they occur depend on field direction. For $\mathbf{H}||[100]$ the CT and OT ramps both end at 39.4 kOe. For $\mathbf{H}||[111]$ the CT and OT ramps end at slightly different fields, 33.4 and 33.7 kOe, respectively.

For OT's in a field parallel to [100] the cubic anisotropy produces an interesting effect. In the absence of anisotropy, the ground level of an OT has a net spin of 7/2. The cubic anisotropy splits the eight-fold degenerate ground level into a doublet, a quartet, and another doublet. This splitting is qualitatively similar to that for singles, except that it is smaller. The low field magnetization for $\mathbf{H}||[100]$ then resembles that of singles (Fig. 1), but the MST occurs at a lower field, near 1.9 kOe instead of 3.4 kOe. This low-field MST for OT's is in addition to the seven MST's at higher fields, between 14.5 and 39.4 kOe.

Because relatively few spins are in triplets, the effects of the cubic anisotropy on the triplets have only a slight influence on the shape of the magnetization curve as a whole. One effect of the anisotropy which was observed experimentally in the present work is the dependence of the end of the triplets' ramp on the direction of $\mathbf{H}$.

B. Other types of anisotropy

The anisotropy arising from the cubic crystal field accounts for the observed behavior of isolated Eu ions (singles), but it cannot explain the splitting of MST's arising from pairs. Such a splitting was observed in the present work. To explain the splitting, three additional anisotropies for pairs were considered. Each of the three can cause pairs with different orientations in the crystal to have MST's at slightly different fields. For example, when $\mathbf{H}$ is parallel to [100] there are two different groups of NN pairs: pairs perpendicular to $\mathbf{H}$, and pairs making a 45° angle with $\mathbf{H}$. These two groups are equivalent in the $1J$-CUB model but are inequivalent when any of the following three additional anisotropies are included: (1) noncubic crystal-field anisotropy; (2) dipole-dipole (DD) anisotropy; and (3) anisotropic exchange.[12–14] As mentioned below, the DD anisotropy can be included formally in the anisotropic exchange, so that it need not be considered separately.

Unlike an isolated Eu ion, each of the two Eu ions in a pair is no longer in a purely cubic crystal-field environment. To describe the changes in the single-ion Hamiltonian $\mathcal{H}_i$ for each of the two Eu ions in the pair, one introduces a coordinate system in which the z axis is along the line joining the two Eu ions. For a NN pair with z along [110], the x axis is along [001], and the y axis along $[1\bar{1}0]$. For a next-nearest-neighbor (NNN) pair with z along [001] the x and y directions are along [100] and [010], respectively. The deviation from cubic symmetry can produce two new terms in $\mathcal{H}_i$, axial and rhombic,

$$\Delta\mathcal{H}_i = D[S_{iz}^2 - (1/3)S(S+1)] + E(S_{ix}^2 - S_{iy}^2). \quad (2)$$

The full single-ion Hamiltonian $\mathcal{H}_i$ also contains the cubic anisotropy, parameterized by b_4 and b_6, and the Zeeman energy.

The possibility of anisotropic exchange is included by taking the exchange interaction in the pair to be of the form[12]

$$\mathcal{H}_{\text{exch}} = -2\bar{J}\mathbf{S}_1\cdot\mathbf{S}_2 - 2D_{\text{exch}}[3S_{1z}S_{2z} - \mathbf{S}_1\cdot\mathbf{S}_2] - 2E_{\text{exch}}[S_{1x}S_{2x} - S_{1y}S_{2y}]. \quad (3)$$

Here, $\bar{J}$ is the average exchange constant, D_{exch} gives the axial anisotropy, and E_{exch} is the rhombic anisotropy in the perpendicular plane. The DD anisotropy can be included in the axial term of Eq. (3) because it has the same form. The effects produced by the anisotropies described by Eqs. (2) and (3) will be discussed later when the splitting of the MST's from pairs is analyzed.

III. EXPERIMENTAL TECHNIQUES

The techniques used to measure the magnetization M were described earlier.[2,3,5] Three magnetometers were used. Measurements above 1.8 K and below 55 kOe, performed primarily for sample characterization, were made with a superconducting quantum interference device magnetometer system manufactured by Quantum Design Inc. Data at 0.6 K in fields up to 180 kOe were obtained with a vibrating sample magnetometer operating in a Bitter magnet. In these 0.6 K experiments the samples were immersed in liquid ^{3}He. The crucial experiments at 20 mK were made in a plastic dilution refrigerator installed in a 50-kOe superconducting magnet. The magnetization at 20 mK was measured with a capacitance force magnetometer.[5] In some of these experiments both dc and ac field gradients were used to produce the force. The two modes of operation gave very similar results. The 20 mK data presented in the figures below were all taken with a dc gradient.

The five $Pb_{1-x}Eu_xS$ samples were grown by the Bridgman method. The Eu concentration x was determined from the saturation magnetization at 0.6 K or 2 K. A spin S = 7/2 for the Eu^{2+} ion, and the EPR value $g = 1.975$, were assumed. The results for the five samples were $x = 0.0092$, 0.026, 0.026, 0.040, and 0.059. To distinguish between the two samples with $x = 0.026$ (obtained from different boules), they will be labeled as sample A and sample B. All values for x were confirmed by the Curie constants which were deduced from susceptibility data between 2 and 100 K.

Magnetization measurements at 20 mK were made only on $x = 0.0092$ and on one of the samples with $x = 0.026$ (sample A). These two single crystals were oriented by x rays, and the magnetization was measured with **H** parallel to the [100] and [111] crystallographic axes. The magnetization of the other three samples (sample B with $x = 0.026$, and the samples with $x = 0.040$ and 0.059) was measured at 0.6 K in fields up to 180 kOe. The orientation of **H** relative to the crystallographic axes was not controlled in these high-field experiments.

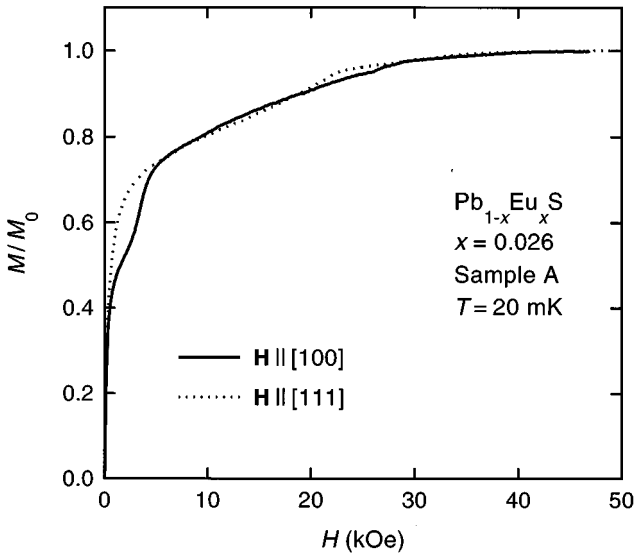

FIG. 3. Magnetization curves for $x = 0.026$ (sample A), measured at $T = 20$ mK with $\mathbf{H}||[100]$ and $\mathbf{H}||[111]$. The magnetization M is normalized to its saturation value M_0.

IV. RESULTS AND DISCUSSION

A. Overall view of the magnetization curves

The overall behavior at 20 mK is illustrated by the results in Fig. 3. The data for $\mathbf{H}||[100]$ show the MST of the singles, near 3.5 kOe. This MST is followed by a ramp arising from pairs, which ends near 29 kOe. The MST of the singles is absent when **H** is parallel to [111]. On the other hand, the pairs' ramp is also observed for $\mathbf{H}||[111]$, except that it ends at a significantly lower field, near 23 kOe. All these features are expected from the 1J-CUB model discussed in Sec. II A. An expanded version of Fig. 3 (not shown) indicates that after the ramp from the pairs ends, there remains a smaller ramp, attributed to triplets. The triplets' ramp ends at a field which depends on field direction, about 34 kOe for $\mathbf{H}||[111]$ and about 40 kOe for $\mathbf{H}||[100]$. At 50 kOe the magnetization is practically saturated.

An example of data at 0.6 K in fields up to 180 kOe is shown in Fig. 4. Similar results were obtained for sample B ($x = 0.026$) and for $x = 0.040$. The ramps which were very distinct at 20 mK are more rounded at 0.6 K. There are no additional ramps or MST's above 50 kOe. The magnetization reaches saturation near 70 kOe. As pointed out later, the Curie-Weiss temperatures for these samples indicate that the dominant exchange constant J is of order -0.1 K. Such a low value of J implies that the saturation observed in Fig. 4

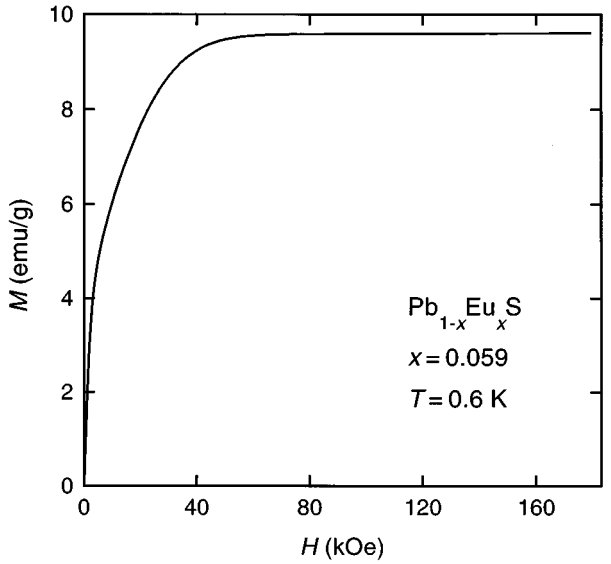

FIG. 4. Magnetization curve for $x=0.059$ at 0.6 K. A (small) correction for the diamagnetism of the lattice is included.

is a true saturation, as distinguished from the apparent (or ''technical'') saturation commonly observed in II-VI DMS's for which J is much larger.[1]

B. MST of singles

A clear view of the MST arising from the singles is shown in Fig. 5. These results, obtained at 20 mK, are for $x=0.0092$ with $\mathbf{H}||[100]$. The data confirm the prediction that this MST results in a factor of 7/5 increase of M. Analysis of the derivative dM/dH shows that for this sample the MST is at $H_c=3.39\pm0.1$ kOe. For $x=0.026$, (sample A) $H_c=3.47\pm0.1$ kOe. Both experimental values agree with the prediction $H_c=3.38$ kOe.

The width of the MST is defined as the full width at half height of the peak in dM/dH. The experimental width is 0.9

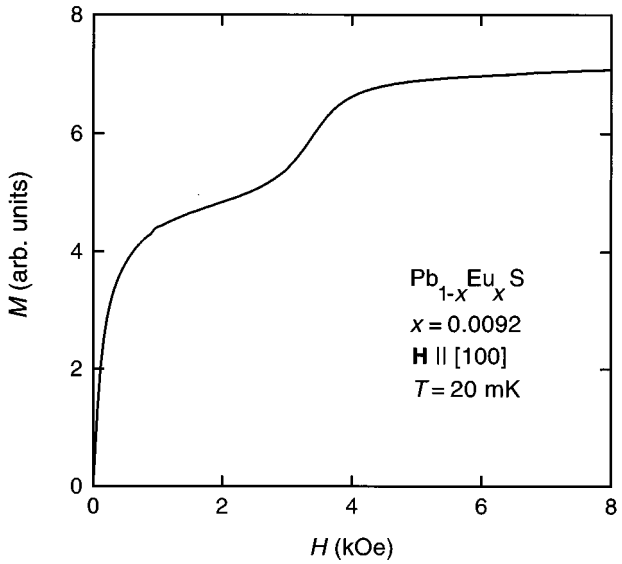

FIG. 5. Low-field portion of the magnetization curve for $x=0.0092$, measured at 20 mK with $\mathbf{H}||[100]$.

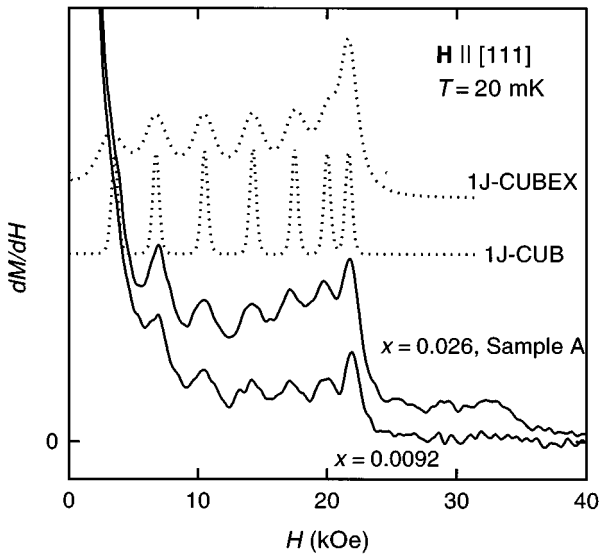

FIG. 6. Experimental results (solid curves) and computer simulations (dotted curves) for dM/dH when $\mathbf{H}||[111]$ and $T=20$ mK. The computer simulations are for pairs only, and are based on the $1J$-CUB and $1J$-CUBEX models. The parameters for the two models are given in the text. The zero of the ordinate scale applies only to the experimental results for both samples. The ordinate scale for different curves is different.

kOe for $x=0.0092$, and 1.2 kOe for $x=0.026$. The calculated thermal width at 20 mK is only 0.5 kOe. The difference between the observed widths and the thermal width is attributed to two causes. First, any misalignment of $\mathbf{H}$ relative to the [100] direction will broaden and shift the MST, as discussed in Ref. 2. A misalignment of 3°, for example, should lower H_c by 0.04 kOe and increase the width by 0.3 kOe. Second, interactions with distant Eu spins should also broaden the MST. By definition, singles have no Eu neighbors to which they are coupled by the dominant exchange constant J. However, there are always distant Eu neighbors to which such singles are coupled by weaker exchange constants. These distant-neighbor interactions should broaden the MST arising from singles, and also shift it slightly, just as they affect the MST's from pairs.[18] As x increases, there are more distant neighbors so that the effects of distance neighbors should increase. The experimental data show that even for $x=0.026$ the effects of distant neighbors are small; the shift in the position is less than about 0.1 kOe, and the additional broadening is no more than 0.7 kOe.

C. Exchange constant

The exchange constant J was determined from the MST's arising from pairs in the configuration $\mathbf{H}||[111]$. The $1J$-CUB model, which gives a good account of the data for $\mathbf{H}||[111]$, was used for this purpose. Later, in Sec. IV E, we will use another model which includes exchange anisotropy in addition to the cubic anisotropy. The value of J will remain the same, but J will then be identified as the average exchange constant $\bar{J}$ in Eq. (3).

Figure 6 shows the derivative dM/dH at 20 mK for $\mathbf{H}||[111]$. These results were obtained numerically from the magnetization curves for the two samples which were stud-

ied at this very low temperature. Following the large values of dM/dH at low fields, due to the alignment of the singles, six MST's are observed at higher fields for each sample. These correspond to the second through seventh MST's from pairs. The first pairs' MST is masked by the large derivative from the singles. Once the seventh MST is completed, the ramp due to the pairs ends and the derivative drops. For $x=0.026$ there is another, smaller, drop of dM/dH near 34 kOe. The position of the latter drop agrees with the calculated ends of the triplets' ramps, which are nearly the same for CT's and OT's. For $x=0.0092$ the percentage of spins which are in triplets is much smaller,[16] so that the end of the triplets' ramp is not observed.

The positions of the dM/dH peaks in Fig. 6 are the same for $x=0.0092$ and 0.026, within about 0.1 kOe. This result indicates that the shifts in the positions of the MST's caused by distant neighbors[18] are small, because such shifts increase with x. A similar conclusion was reached earlier for the MST arising from singles. It follows that models which include only the dominant J are adequate for describing the positions of the MST's.

The value of the exchange constant J is determined by matching the observed MST's from pairs with simulations using the $1J$-CUB model. The simulations, which are for pairs only, use the EPR values for the crystal field parameters and the g factor. The only adjustable parameter is J. A reasonably good match is obtained with $J/k_B=-0.228$ K, as shown in Fig. 6. The match becomes unsatisfactory if J is changed by more than 3%. Thus, $J/k_B=-0.228\pm0.007$ K.

The value of J quoted above corresponds to the largest AF exchange constant. If a larger AF exchange constant existed it would have resulted in additional pairs' ramps (consisting of MST's) in fields above those of the main ramp in Fig. 3. Such pairs' ramps would have been recognized easily. The absence of additional ramps or MST's up to 50 kOe (Fig. 3) places a lower limit of 4 K on the magnitude of any larger AF exchange constant. Using the data in Fig. 4, up to 180 kOe, the lower limit increases to 12 K. Exchange constants above 12 K are incompatible with the Curie-Weiss temperatures of these samples. The Θ's were deduced from susceptibility data, obtained with the SQUID magnetometer. All the Θ's were negative. A standard analysis which assumed one dominant exchange constant[19] indicated that this exchange constant is AF and is of order -0.1 K. This result is consistent with the value -0.228 K deduced from the MST's.

D. Identification of J

In EuS, EuSe, and EuTe the largest AF exchange constant is $J_2\equiv J_{\rm NNN}$, for next-nearest neighbors (NNN's).[20] On the other hand, in $Pb_{1-x}Eu_xSe$ and $Pb_{1-x}Eu_xTe$ (with low x) it was found that the NN exchange constant $J_1\equiv J_{\rm NN}$ is the largest AF exchange constant.[2,3] The following analysis indicates that the AF exchange constant J determined in the preceding section also is J_1.

The identification of J is based on comparisons between the measured magnetization curves and computer simulations which start from two competing hypotheses: (1) J is J_1 and all other exchange constants, including J_2, vanish, or (2) J is J_2 and all other exchange constants, including J_1, vanish. The predictions based on the two hypotheses are very different essentially because there are 12 NN cation sites but only 6 NNN cation sites. The main assumption in the simulations is that the Eu ions are randomly distributed over the cation sites.

The simulations in Ref. 2 included only singles, pairs, and triplets. In a later work,[3] the relatively small contributions from quartets[15] and larger clusters were also included. In the present work too the simulations take into account quartets and larger clusters. But in contrast to the earlier simulations which neglected the anisotropy, some of the present simulations include an approximation for the anisotropy.

The choice of J as J_1 or J_2 does not fully specify the simulation. It is also necessary to specify the model for the anisotropy. In the present section the simulations are for (1) experiments at 20 mK on oriented samples, and (2) measurements at 0.6 K on unoriented samples. The simulations of the 20 mK data use the $1J$-CUB model for singles, pairs, and triplets, but quartets and larger clusters are treated using the simpler $1J$-0 model (no anisotropy). For the samples which were measured at 20 mK ($x\leqslant0.026$), no more than 2.2% of the spins are in quartets or larger clusters, so that the $1J$-CUB model is used for practically all the spins.

The simulations of the 0.6 K data use the $1J$-0 model throughout because the field direction is unknown. Actually, the differences between simulations which include the anisotropy and those which ignore it, or between simulations with different models for the anisotropy, are small compared to the difference between choosing J as J_1 or J_2. Thus, the identification of J is not affected by the choice of the model for the anisotropy.

Figure 7 shows the simulations of the 20 mK data for $x=0.026$. (To account for nonthermal broadening of the MST's, these particular simulations used an effective temperature of 50 mK. See Ref. 21.) The experimental data in Fig. 7 are the same as in Fig. 3. Quite a good agreement with the simulations is obtained with the choice $J=J_1$. With $J=J_2$ the agreement is poor. A similar result was also obtained from simulations of the 20 mK data for $x=0.0092$.

Simulations of all the magnetization curves at 0.6 K confirmed the choice $J=J_1$. For two of the three samples ($x=0.059$, and sample B with $x=0.026$) the agreement with the J_1 simulations is excellent, as shown in Fig. 8. For the third sample ($x=0.040$) there is a slight difference between the data and the J_1 simulation, comparable to the difference in Fig. 7, but the overall agreement is still quite good. Based on all the simulations J is identified as the NN exchange constant J_1.

The key assumption in the simulations is that the Eu distribution is random. The simulations are sensitive to deviations from this assumption. The good-to-excellent agreement with the J_1 simulations implies that the Eu distribution in these $Pb_{1-x}Eu_xS$ crystals was random or very close to random. Significant deviations from the J_1 simulations were found in the earlier work on $Pb_{1-x}Eu_xTe$.[3] They were attributed to departures from a random distribution.

E. Splitting of MST's from pairs, for H||[100]

For $\mathbf{H}||[100]$, detailed studies of the pairs' magnetization ramp at 20 mK revealed an unanticipated structure. Figure 9

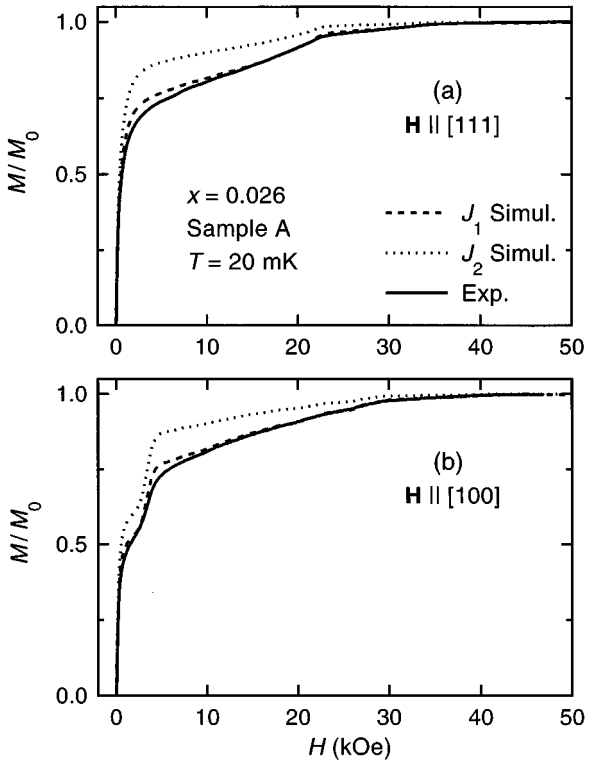

FIG. 7. Comparison between the magnetization curves in Fig. 3, measured at 20 mK, with computer simulations which assume that J is either J_1 or J_2. (a) Results for $\mathbf{H}||[111]$. (b) Results for $\mathbf{H}||[100]$. The computer simulations use the $1J$-CUB model for singles, pairs, and triplets, but the $1J$-0 model for larger clusters. The magnetization M is normalized to its saturation value M_0.

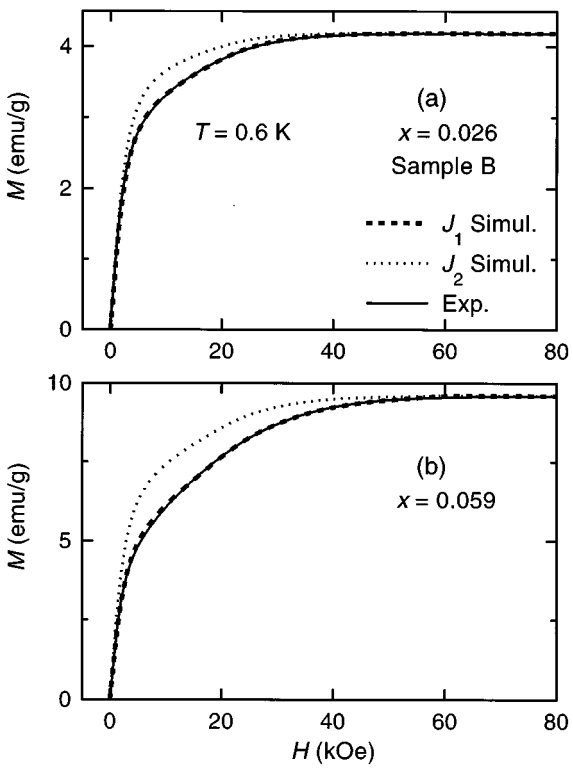

FIG. 8. Comparison between magnetization curves measured at 0.6 K with computer simulations which assume that J is either J_1 or J_2. (a) Results for $x=0.026$ (sample B). (b) Results for $x=0.059$. The computer simulations use the $1J$-0 model for all the clusters.

shows the results for $x=0.0092$. There are more steps in this figure than the seven expected from either the $1J$-0 or the $1J$-CUB models. The larger number of steps is seen more clearly in the derivative dM/dH of these data, shown in Fig. 10 (lowest curve). Results of a detailed study of the pairs' ramp in sample A ($x=0.026$) are also shown in Fig. 10. There is good agreement between the dM/dH spectra from the two samples. The peaks in dM/dH suggest that each of the seven MST's predicted by the simple models is split into two.

A splitting of the MST's may be caused by two slightly different AF exchange constants, with different neighbors. This possibility was rejected based on computer simulations with two exchange constants, which failed to reproduce the experimental dM/dH curves in Fig. 10. Two exchange constants are also inconsistent with the overall shape of each of the magnetization curves, which depends on cluster statistics. The simulations in Figs. 7 and 8 show good agreement assuming J_1 only. This agreement is ruined if two nearly equal exchange constants, such as J_1 and J_2, are included in the simulations.

The interpretation of the observed pattern in Fig. 10 is based on the existence of two inequivalent groups of NN pairs when $\mathbf{H}$ is along the $[100]$ direction. The pairs in one group, called α, lie in the (100) plane, perpendicular to $\mathbf{H}$. The pairs in the second group, called β, are oriented at a 45° angle to $\mathbf{H}$. The ratio between the numbers of pairs in the two groups is $N_\beta/N_\alpha=2$. It is noteworthy that for $\mathbf{H}||[100]$ there are also two groups of NNN pairs: group α' with pairs parallel to $\mathbf{H}$, and group β' perpendicular to $\mathbf{H}$, with $N_{\beta'}/N_{\alpha'}=2$. The basic idea is to attribute the last doublet in Fig. 10, at the highest fields, to the two groups of pairs. The

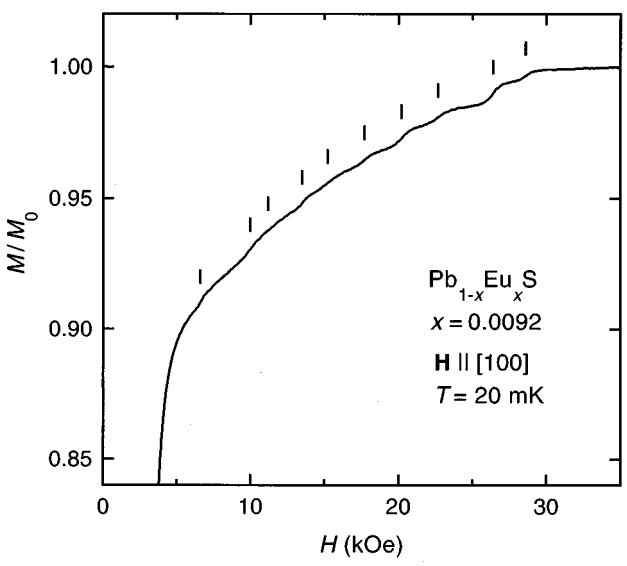

FIG. 9. Expanded view of the pairs' magnetization ramp for $x=0.0092$, measured at 20 mK with $\mathbf{H}||[100]$. The magnetization M is normalized to its saturation value M_0. The locations of the magnetization steps (from the peaks in the lowest curve in Fig. 10) are indicated.

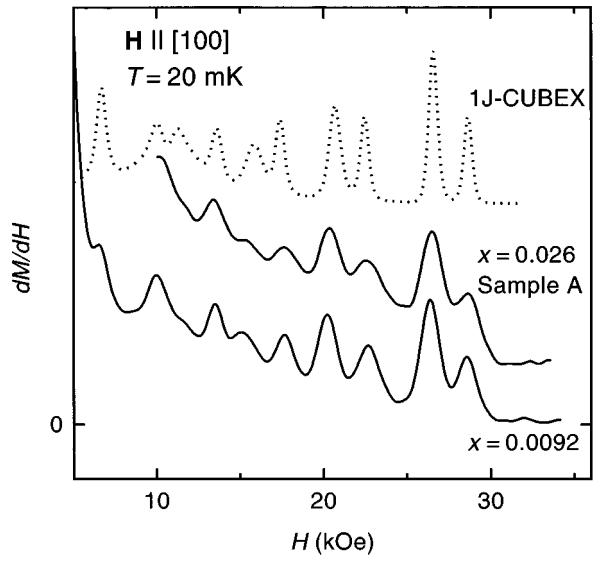

FIG. 10. Experimental results (solid curves) and a computer simulation (dotted curve) for dM/dH when $\mathbf{H}||[100]$ and $T=20$ mK. The computer simulation is for pairs only, and is based on the $1J$-CUBEX model. The parameters for the model are given in the text. The zero of the ordinate scale applies only to the experimental curve for $x=0.0092$. The ordinate scale for different curves is different.

less intense member of this doublet, at the higher field, is attributed to group α (or α'), and the more intense member to group β (β'). The correct pair Hamiltonian, applied to the two groups, should reproduce the entire pattern of the dM/dH peaks, both the splittings and the intensities. The pattern observed in the orientation $\mathbf{H}||[111]$, shown in Fig. 6, should also be reproduced, taking into account inequivalent pairs for that field direction. The pair Hamiltonians which were considered used the anisotropies discussed in Sec. II.

The first attempt was to add the DD interaction (calculated with the lattice constant $a=5.936$ Å of PbS) to the cubic crystal-field anisotropy. It was found that the splitting produced by the DD interaction alone is far too small. In the second attempt the noncubic crystal field terms given by Eq. (2), and also the DD interaction, were added to the cubic anisotropy. An extensive study failed to find values of D and E which would lead to a good match with the dM/dH spectra if J is the NN exchange constant J_1. A reasonably good match was found, with a purely axial anisotropy ($E=0$), if one assumed that J was the NNN exchange constant J_2. However, the evidence that J is J_1 is very strong, as discussed in Sec. IV D. Figures 7 and 8, presented in that section, show a good match between the magnetization curves and simulations which use J_1 and a random distribution of Eu ions. To obtain a match with the observed magnetization curves using J_2 would have required a very nonrandom distribution of Eu ions, with just the right nonrandomicity. The possibility of such a coincidence for five different samples is extremely remote, and it was therefore rejected.

More satisfactory results were obtained by adding the exchange anisotropy given by Eq. (3) to the cubic crystal-field anisotropy. This model will be called the $1J$-CUBEX model. The DD interaction is included in the axial term of the exchange anisotropy. A reasonably good match with the dM/dH spectra was obtained with several combinations of parameters, assuming NN pairs. One of the best choices is $\overline{J}/k_B=-0.228$ K, $D_{\rm exch}/k_B=0.017$ K, and $E_{\rm exch}/k_B=-0.034$ K. The pair spectrum for $\mathbf{H}||[100]$ calculated using these parameters is shown in Fig. 10. The calculated pair spectrum for $\mathbf{H}||[111]$ is shown in Fig. 6. (For $\mathbf{H}||[111]$ also there are two inequivalent groups of NN's, which lead to a splitting of the MST's. However, the splitting for this field orientation is so small that it is not seen in the simulation at 20 mK.) Both in Fig. 6 and in Fig. 10 there are small deviations between the calculated and observed spectra. For example, in Fig. 6 the observed separation between the two peaks at the highest fields is not well reproduced by the model. However, the overall agreement is quite good.

A variety of values for the three parameters of the $1J$-CUBEX model was tried. The uncertainty in the value $\overline{J}/k_B=-0.228$ K quoted above is only 3%. (It is noteworthy that the value and uncertainty for $\overline{J}$ are the same as those for J in Sec. IV C.) There is considerably more freedom in choosing the values of $D_{\rm exch}$ and $E_{\rm exch}$. Some combinations in which $D_{\rm exch}$ and $E_{\rm exch}$ are changed by up to 50%, relative to the values given above, fit the experimental data nearly equally well. The value $D_{\rm exch}/k_B=0.017$ K quoted above is close to that calculated from the DD interaction alone, but $E_{\rm exch}$ must be attributed to exchange anisotropy. It may be possible to improve the agreement with the data by adding the noncubic crystal field terms of Eq. (2) to the model. However, since the model will then involve five adjustable parameters, this approach was not pursued.

Normally, exchange anisotropy for S-state ions such as Eu^{2+} is very small. In contrast, the value of $E_{\rm exch}$ found here is a sizable fraction of $\overline{J}$. Of course the fact that we were unable to account for the pattern of the splitting of the MST's without invoking exchange anisotropy is no guarantee that there is no other explanation for it. For this reason the interpretation in terms of exchange anisotropy is still viewed as tentative. In contrast, the conclusions concerning the value of the dominant exchange constant $\overline{J}$, its identity as J_1, and the random distribution of the Eu ions, are viewed as firm.

F. Conclusion

To conclude, we summarize our results on a series of lead chalcogenides with a small concentration of Eu. For the three compounds studied, all with $x<0.06$, we have found that J_1 is the leading antiferromagnetic exchange constant. The measured values are $J_1/k_B=-0.228\pm0.007$ K for $Pb_{1-x}Eu_xS$ (this work), $J_1/k_B=-0.24\pm0.03$ K for $Pb_{1-x}Eu_xSe$, and $J_1/k_B=-0.264\pm0.018$ K for $Pb_{1-x}Eu_xTe$.

The exchange constants in the corresponding Eu chalcogenides ($x=1$) are very different. For EuS, EuSe, and EuTe the largest AF exchange constant is J_2, while J_1 is ferromagnetic.[20] Despite sharing the same rock salt structure, the pure Eu chalcogenides and the corresponding IV-VI

DMS's have very dissimilar electronic band structures. The positions of the $4f^7$ levels of the Eu^{2+} ion may also be different. Thus, the observed differences in the Eu-Eu exchange constants are not so surprising. While the exchange mechanisms in the pure Eu-chalcogenides are well understood theoretically, this is not the case for the DMS's.

ACKNOWLEDGMENTS

The work in Brazil was supported by CNPq, FAPESP, and FINEP. The work in the U.S. was partially supported by NSF. The work in France was supported by CNRS. The work in Poland was supported by Grant No. 2 P03B 091 12 of the Polish Committee for Scientific Research.

[1] Y. Shapira, J. Appl. Phys. **67**, 5090 (1990); in *Semimagnetic Semiconductors and Diluted Magnetic Semiconductors*, edited by M. Averous and M. Balkanski (Plenum, New York, 1991).

[2] V. Bindilatti, N.F. Oliveira, Jr., Y. Shapira, G.H. McCabe, M.T. Liu, S. Isber, S. Charar, M. Averous, E.J. McNiff, Jr., and Z. Golacki, Phys. Rev. B **53**, 5472 (1996).

[3] E. ter Haar, V. Bindilatti, N.F. Oliveira, Jr., G.H. McCabe, Y. Shapira, Z. Golacki, S. Charar, M. Averous, and E.J. McNiff, Jr., Phys. Rev. B **56**, 8912 (1997).

[4] G. Bauer and H. Pascher, in *Diluted Magnetic Semiconductors*, edited by M. Jain (World Scientific, Singapore, 1991).

[5] V. Bindilatti, N.F. Oliveira, Jr., E. ter Haar, and Y. Shapira, Czech. J. Phys. **46**, Suppl. 6, 3255 (1996); V. Bindilatti and N.F. Oliveira, Jr., Physica B **194-196**, 63 (1994).

[6] T.Q. Vu, V. Bindilatti, Y. Shapira, E.J. McNiff, Jr., C.C. Agosta, J. Papp, R. Kershaw, K. Dwight, and A. Wold, Phys. Rev. B **46**, 11 617 (1992).

[7] W.J.M. de Jonge and H.J.M. Swagten, J. Magn. Magn. Mater. **100**, 322 (1991).

[8] H.J.M. Swagten, C.E.P. Gerrits, A. Twardowski, and W.J.M. de Jonge, Phys. Rev. B **41**, 7330 (1990).

[9] V. Bindilatti, A.N. Anisimov, N.F. Oliveira, Jr., Y. Shapira, M. Goiran, F. Yang, S. Isber, M. Averous, and M. Demianiuk, Phys. Rev. B **50**, 16 464 (1994); S. Isber, M. Averous, Y. Shapira, V. Bindilatti, A.N. Anisimov, N.F. Oliveira, Jr., V.M. Orera, and M. Demianiuk, *ibid.* **51**, 15 211 (1995).

[10] G.H. McCabe, Y. Shapira, V. Bindilatti, N.F. Oliveira, Jr., A. Twardowski, W. Mac, E.J. McNiff, Jr., and M. Demianiuk, Solid State Commun. **95**, 841 (1995).

[11] G.B. Bacskay, P.J. Fensham, I.M. Ritchie, and R.N. Ruff, J. Phys. Chem. Solids **30**, 713 (1969); S. Isber, Ph.D. thesis, University of Montpellier II, 1996.

[12] J. Owen and E.A. Harris, in *Electron Paramagnetic Resonance*, edited by S. Geschwind (Plenum, New York, 1972).

[13] J. Owen, J. Appl. Phys. **32**, 213S (1961).

[14] B.A. Calhoun and J. Overmeyer, J. Appl. Phys. **35**, 989 (1964).

[15] M.T. Liu, Y. Shapira, E. ter Haar, V. Bindilatti, and E.J. McNiff, Jr., Phys. Rev. B **54**, 6457 (1996).

[16] R.E. Behringer, J. Chem. Phys. **26**, 1504 (1957); M.M. Kreitman and D.L. Barnett, *ibid.* **43**, 364 (1965). See also Ref. 15.

[17] A. Abragam and B. Bleaney, *Electron Paramagnetic Resonance of Transition Ions* (Dover, New York, 1986), Secs. 3.4 and 5.9.

[18] B.E. Larson, K.C. Haas, and R.L. Aggarwal, Phys. Rev. B **33**, 1789 (1986).

[19] J. Spalek, A. Lewicki, Z. Tarnawski, J. K. Furdyna, R. R. Galazka, and Z. Obuszko, Phys. Rev. B **33**, 3407 (1986).

[20] A. Mauger and C. Godart, Phys. Rep. **141**, 51 (1986); P. Wachter, in *Handbook on the Physics and Chemistry of Rare Earths*, edited by K.A. Gschneidner, Jr. and L. Eyring (North Holland, Amsterdam, 1979), Vol. I, p. 507 ff.

[21] In the $1J$-CUB and $1J$-0 models, thermal broadening is the sole cause of the finite widths of the MST's. One difficulty in simulating the 20 mK data is that the observed widths are larger than the thermal width. This can be seen in Fig. 6 by comparing the experimental widths with those in the $1J$-CUB simulation. Among the reasons for the larger observed widths in Fig. 6 is an unresolved splitting of the MST's (Sec. IV E). Another reason is the interaction with distant neighbors (Ref. 18). To account for the larger widths, the simulations of the 20 mK data in Fig. 7 assume an effective temperature of 50 mK. This change merely smoothes some sharp features in the simulated curves, but has no influence whatsoever on the identification of J. The simulations of the 20 mK data in Figs. 6 and 10 use the actual temperature. The simulations of the 0.6 K data in Fig. 8 also use the actual temperature because at this higher temperature thermal broadening dominates.